

Evaluation of the physical characteristic of Cerrobend blocks used for radiation therapy

A. Taherkhani¹, M. Mohammadi^{2,3*}, M.S. Saboori⁴, V. Changizi⁵

¹Department of Biophysics, Science & Research Campus, Azad University, Tehran, Iran

²Department of Medical Physics, Faculty of Medicine, Hamadan University of Medical Sciences, Hamadan, Iran

³Department of Medical Physics, Royal Adelaide Hospital, and School of Chemistry and Physics, The University of Adelaide, Adelaide, SA, 5000, Australia

⁴Department of Medical Physics, Faculty of Medicine, The University of Erlangen, Erlangen, Germany

⁵Department of Medical Physics, Tehran University of Medical Sciences, Tehran, Iran

Background: In Radiation Therapy, the sparing of normal tissues can be performed using either multi-leaf collimators or Cerrobend blocks. The current work focuses on the physical characteristics of Cerrobend blocks including attenuation coefficient, effective penumbra width and isodose curves undulation in penumbral regions. **Materials and Methods:** All measurements were performed using a dual energy linac and the Cerrobend blocks designed and fabricated using a commercial Cerrobend material. Data were collected using a calibrated ionization chamber as well as EDR2 films. **Results:** The results showed that the attenuation coefficient was found to be 0.4475 and 0.4276 cm⁻¹ for photon beams 6MV and 15 MV, respectively, and a potential air bubble with a diameter greater than 3 mm affects beam attenuation significantly. The optimum Cerrobend block width was found to be around 16 mm. The isodose curves scalloping achieved for secondary collimator jaws, were also similar. **Conclusion:** If Cerrobend blocks are used as a basic method to protect normal tissues, its physical characteristics will be recommended to be taken into account comprehensively. *Iran. J. Radiat. Res., 2010; 8 (2): 93-101*

Keywords: Beam collimation, block-cutter, Cerrobend blocks, shielding.

INTRODUCTION

In radiation therapy, regarding hazardous effects of radiation for healthy tissues surrounds tumoral tissues; the protection of normal tissues is essential (1, 2). The protection of normal tissues can be performed by the collimating of radiation beam. For irregular radiation fields, either Cerrobend blocks (3-7) or MmultiLeaf collimators (MLCs) (8-16) can be used.

MLCs as extra-accessories are mounted

in medical linear accelerators (linacs) head. The MLCs are basically controlled by computers. The main advantages of MLCs are: the saving of treatment time, the possibility of treatment information transfer, and providing a clean environment (8, 10, 17, 18). However, MLCs are not only too expensive, but they are also more complicated; it is preferred to use conventional methods to protect organ at risks (OARs), and normal tissues in developing countries. They are not too expensive and regardless of the complicated software and computer dependency, radiation beam can easily be shaped using a simple machine. There is also no serious concern for interleaf and intraleaf leakages routinely can be addressed as one of the main disadvantages of MLCs (14, 17, 19-27). In addition the penumbra regions created using MLCs are generally reported to be larger than those generated by Cerrobend blocks (10-16, 28-33).

The thickness of Cerrobend blocks strongly depends on the main substance chemical formula, block maker furnace temperature and environmental conditions (7). Most of studies and guidelines have mentioned that a 7 to 8 cm thickness of a Cerrobend block is enough to protect normal tissues(1, 2). There is no evidence that more thick Cerrobend blocks, for instance 9 or 10 cm, are evaluated. In addition, dose distribution in protected area strongly

*Corresponding author:

Dr. Mohammad Mohammadi,

Department of Medical Physics, Royal Adelaide Hospital, Adelaide, South Australia 5000, Australia.

Fax: +61 82225937

E-mail: mohammadi@umsha.ac.ir

depends on the Cerrobend blocks shapes. Regarding the establishment of MLCs in most of radiotherapy research centers, this important factor is also not investigated.

This study focused on the Cerrobend blocks attenuation and the impact of air bubbles can potentially be happened during block molding, as well as physical characteristics of Cerrobend blocks such as the optimum thickness of blocks, utilized for clinical purposes. In addition, as physical characteristics of Cerrobend blocks, the optimum width of a typical Cerrobend block, as well as the dose distribution in penumbra region for a range of Cerrobend blocks were investigated.

MATERIALS AND METHODS

All measurements were performed using a Primus linac (Siemens, Germany) established in the Mahdiah Radiotherapy and Oncology, Hamadan, Iran. The primus linac provides two low and high energy photon beams (6 and 15 MV) and a range of electron beams. All blocks are used in the current study were designed and fabricated by a commercial Cerrobend material, routinely used for clinical purposes.

Evaluation of Cerrobend block attenuation coefficient

A scenario, shown in figure 1, was developed to measure Cerrobend block attenuation coefficient. A calibrated ionization chamber was positioned at the build-up layer and a $1 \times 1 \times 10 \text{ cm}^3$ Cerrobend block mounted on a commercial plexiglass tray was put in tray position, routinely used for clinical purposes. Two consecutive exposures were performed and the average was calculated. The Cerrobend block thickness were then increased 1 cm up to 10 cm. In order to control the back scattering; a 10-centimeter-thick water equivalent material was also put behind the ionization chamber.

Evaluation of a Cerrobend block optimum width

In order to investigate the optimum

Cerrobend block width, a typical Cerrobend block was designed. This is shown in figure 2. Two-dimensional dose distributions were investigated using Kodak Extended Dose Range (EDR2) radiographic films, sandwiched between RW3 slabs at the build-up layer, as well as in a 10-cm depth. The EDR2 films were found to be approximately energy independence in a wide range of radiation dose⁽³⁴⁻³⁹⁾. A 200 cGy at the build-up layer which corresponds to 200 Monitor Units were then delivered, using low and high energy photons. In order to digitalize data acquired and relative dose values, the exposed films were then processed using an automatic film processor (Gevamatic 110 Agfa – Gevarel), and were scanned using a commercial film scanner (Scan maker 9800XL). The dose maps achieved were finally evaluated using in-house codes written in MATLAB.

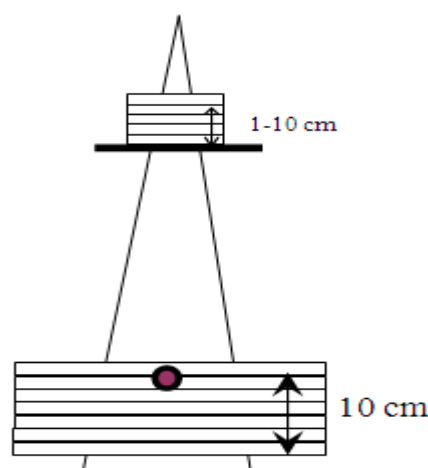


Figure 1. Experiment scenario performed to evaluate Cerrobend block attenuation coefficient.

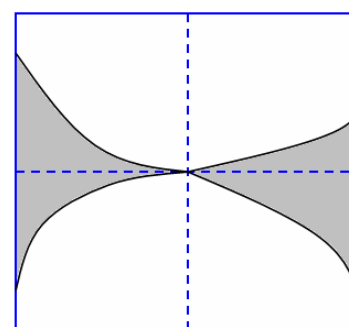


Figure 2. A typical Cerrobend block used to evaluate optimum width of Cerrobend blocks.

Evaluation of penumbra region protected using Cerrobend blocks

In order to investigate dosimetric and physical characteristics of radiation field penumbra region protected using Cerrobend blocks, two typical blocks were designed. These are shown in figure 3. In order to investigate undulation of isodose curves in penumbra region, several edge and corners were designed in a Cerrobend block as shown in figure 3 (a). The results of this block can be compared with similar studies performed using MLC leaf penumbra regions. The second blocks were designed to evaluate characteristics of internal and external penumbra regions compared to those achieved using collimator jaws. Data acquisition procedures were the same as described for the Cerrobend block optimum width.

RESULTS AND DISCUSSION

Evaluation of the attenuation coefficient of Cerrobend blocks

Results of radiation beam attenuation for photon 6MV and 15MV are shown in figures 4 (a) and 4(b), respectively. The x

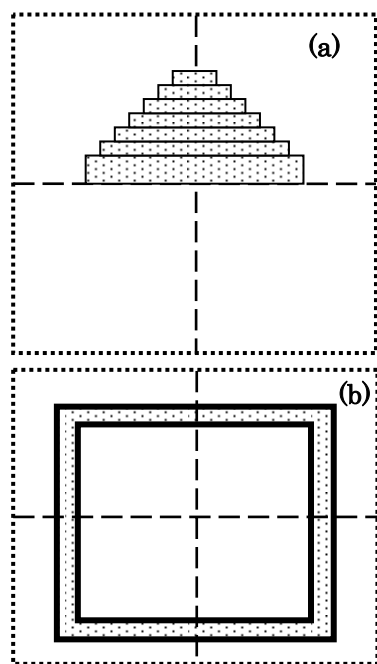


Figure 3. Typical Cerrobend blocks designed to evaluate (a) isodose undulation, (b) internal and external width of radiation field penumbral region.

and y axes represent the average relative ionization chamber reading and Cerrobend block thickness, respectively. An exponential decrease of chamber reading was observed. The results showed that regardless several fluctuations, the measurements were found to be in agreement with curve fitting with $R^2 = 0.9974$ and 0.9985 for Photons 6MV and 15MV, respectively.

Using the corresponding formula, achieved by curve fitting, the attenuation coefficient was found to be 0.4475 and 0.4276 cm^{-1} for photon beams 6MV and 15 MV, respectively. The discrepancy between attenuation coefficients shows that the attenuation factor was strongly dependant on the beam energy and beam hardening; therefore, it should have been taken into account. The Half Value Thickness (HVT) and five HVT (5HVT) are important factors can then be computed, using attenuation coefficient. This is shown in table 1.

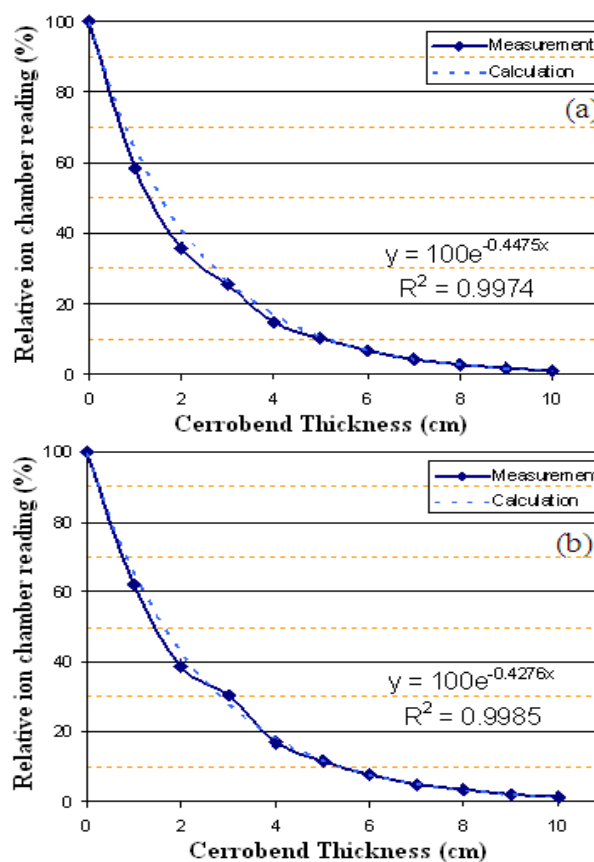


Figure 4. Attenuation of photon beam intensity with the variation of Cerrobend block thickness for (a) 6MV and (b) 15 MV photons.

Table 1. Half Value Thickness and Five Half Value thickness for Cerrobend blocks.

Photon Energy	Half Value Thickness (HVT) (cm)	Five Half Value Thickness (5HVT) (cm)
6 MV	1.549	7.745
15 MV	1.621	8.105

The main reason of the fluctuation of attenuation curves seems to be: the fluctuation of ionization chamber reading which was within 1%, as well as the fluctuation of the Cerrobend block thickness due to the possible air bubbles. The typical air bubble, observed in the Cerrobend blocks have been used in the current study, is shown in figure 5. This evaluation showed that an air bubble with a diameter larger than 3 mm could affect beam attenuation significantly. The air bubble effect, occurred in a 3-cm thick Cerrobend block, is also can be observed in figure 4.

Although a Three Tenth Value Thickness (3TVT), which is able to reduce the beam intensity into 0.1% of primary intensity, is recommended to be used for primary radiation protection, the current study indicated that a 3TVT the Cerrobend block thickness in radiation beam path should be around 15.44 and 16.15 cm for photon 6MV and 15 MV, respectively. Regarding space limitation in linac head, this has been impossible, and under the current situation, at least 3% of primary beam intensity could be passed from conventional Cerrobend thicknesses ⁽⁹⁾.

Evaluation of Cerrobend block optimum width

Two-dimensional relative dose distributions, measured by using EDR2 film for a 6MV photon measured at the build up layer and in a 10-cm depth, are shown in figure 5. In addition, the important part of radiation dose map, is zoomed. The x and y axes are dose map pixel numbers. The irradiated and protected areas are shown in red and blue, respectively. The zoomed dose maps indicated that in the central part of radiation beam, where two narrow Cerrobend blocks met each other, the dose measured was much higher than the attenuated beam

discussed previously. As figures a2 and b2 show, the doses delivered in the central area exceeded 60% for both photon energies. This observation showed that a minimum Cerrobend width is required to spare protected areas.

More details for low energy and high photons (6 MV and 15 MV) are shown in figure 6. In this figure, several arrows are plotted and the corresponding length for each arrow is measured using each corresponding pixel size in the scanned files. Using the lengths of these arrows, one will be able to indicate the relationship between Cerrobend block width and the relative dose distribution in the protected area which is typically shown in figure 7.

Figure 7 shows that the optimum width for a typical Cerrobend block strongly depends on the photon beam energy, as well as on the depth of interest. Although for making of Cerrobend blocks these kinds of details are not necessary, medical physicists and radiation oncologist are recommended to have a reasonable background about dose distribution in different depths for irradiated and protected areas. This is an important issue where an OAR is located in the protected area, and it is supposed to be shielded by using a Cerrobend block perfectly. As figure 7 shows, in order to achieve a reasonable dose for protected area, for instance less than 20%, the Cerrobend block width should be around 16 mm.

Evaluation of penumbra region protected using Cerrobend blocks

Typical relative dose distribution maps for a stepped shaped Cerrobend block, whose structure is shown in figure 3(a), for 6MV and 15 MV photons are shown in figure 8. Like other dose maps which are illustrated previously, the irradiated and protected areas are shown in red and blue,

respectively. The dosimetric characteristics of penumbra regions in zoom are also shown in figure 9.

Evaluation of isodose curves at penumbra region showed that with an increase of depth of interest, penumbra width was developed. This could be shown for 80% and 10% isodose curves, achieved for photon 6MV (see figure 9 a, b). A decrease of the isodose undulation can also be observed with the increase of the depth of interest. For isodose curves acquired using photon 15 MV, the penumbra width was found to be narrower than those measured for photon 6MV at the same depths. More scalloping was observed for 70% to 20% isodose curves. Compared with similar studies performed by using MLCs, the width of the penumbra region achieved in the current study was found to be around 2-3 mm narrower than those achieved using a MLC block (10-16, 28, 31, 32, 40).

The comparison of penumbra region

characteristics achieved by using Cerrobend blocks with those generated using conventional collimators mounted in linac head is shown in figure 10. This investigation showed that the shape of penumbral region of conventional collimators mounted in linac head were in a routine shape and order.

Although a significant difference in penumbra region was observed for those fields created using Cerrobend blocks and linac secondary collimation tools, it was reported that the MLC penumbra width was slightly wider (1-3 mm) than the penumbra of a radiation field generated using the conventional collimator jaws (10, 13, 23, 24, 41).

As penumbra width was a function of radiation field size, with an increase of radiation field, an increase of penumbra width was expected. As figure 10 shows, a gentle growth of penumbra region for conventional jaws could be addressed. The main cause of the discrepancy was the beam divergency.

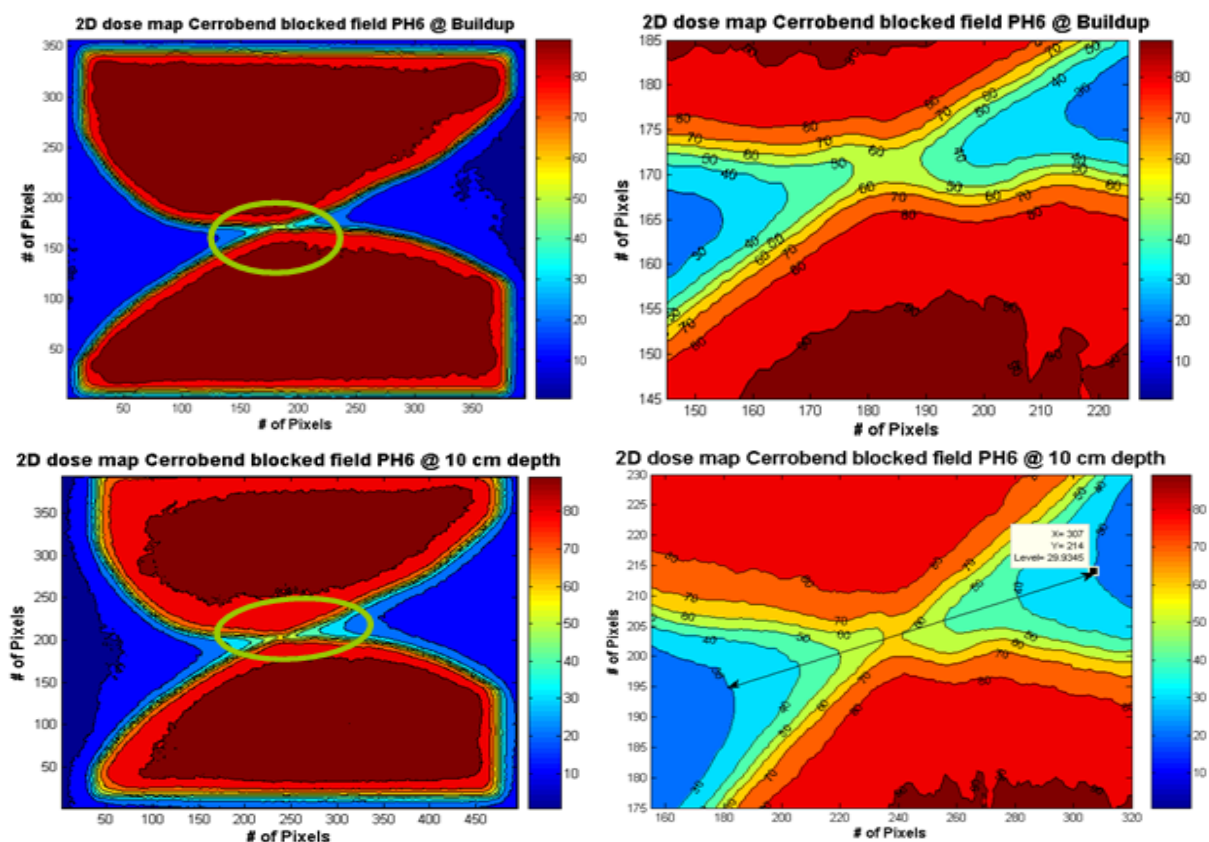


Figure 5. Relative two-dimensional dose distribution for a 6 MV photon, acquired at (a1) build-up layer and (b1) at a 10-cm depth and (a2 & b2) the corresponding magnified critical areas shielded using a typical Cerrobend block.

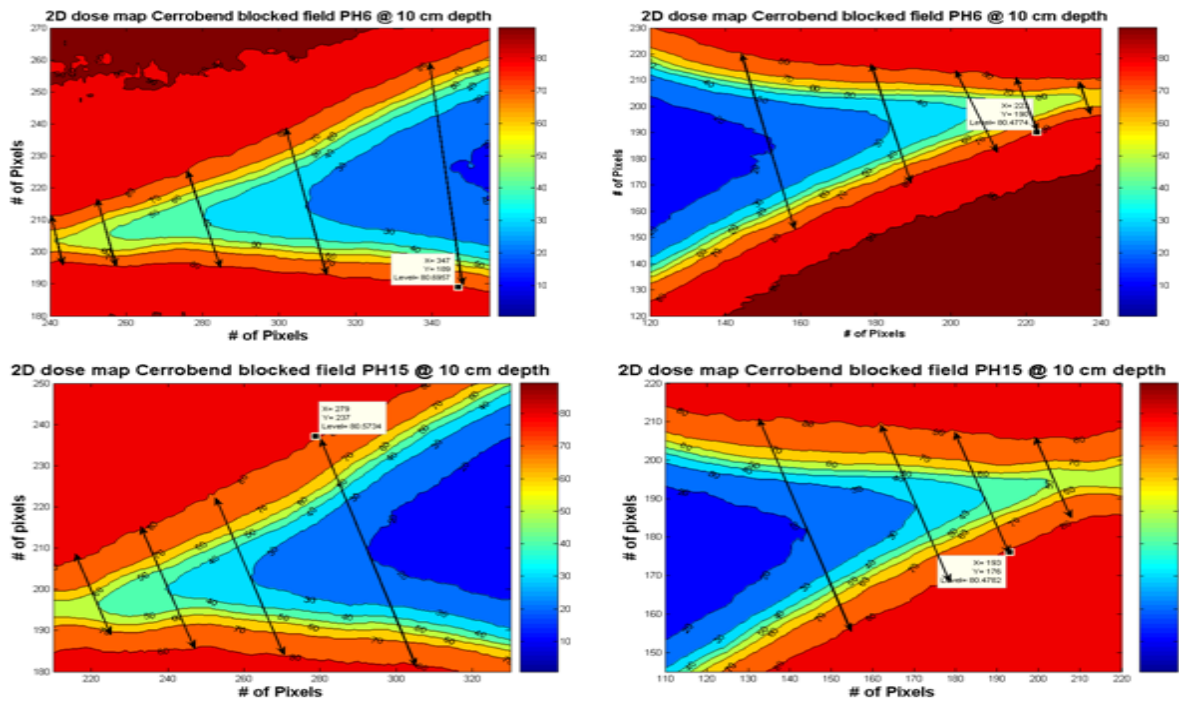


Figure 6. Typical zoomed two-dimensional dose distributions for radiation fields shielded using a typical Cerrobend block measured at 10 cm depth of a homogenous phantom for (a1 and a2) low energy, and (b1 and b2) high energy photons.

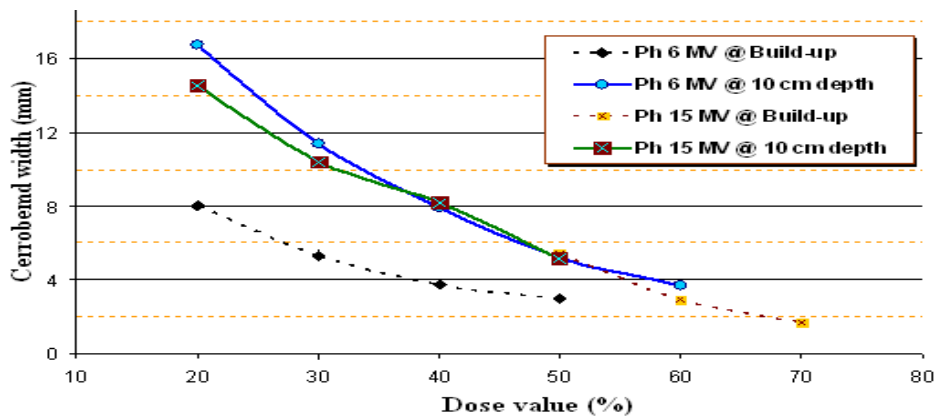


Figure 7. The relationship between dose values delivered at the build up layer and at 10 cm depth and the Cerrobend block width.

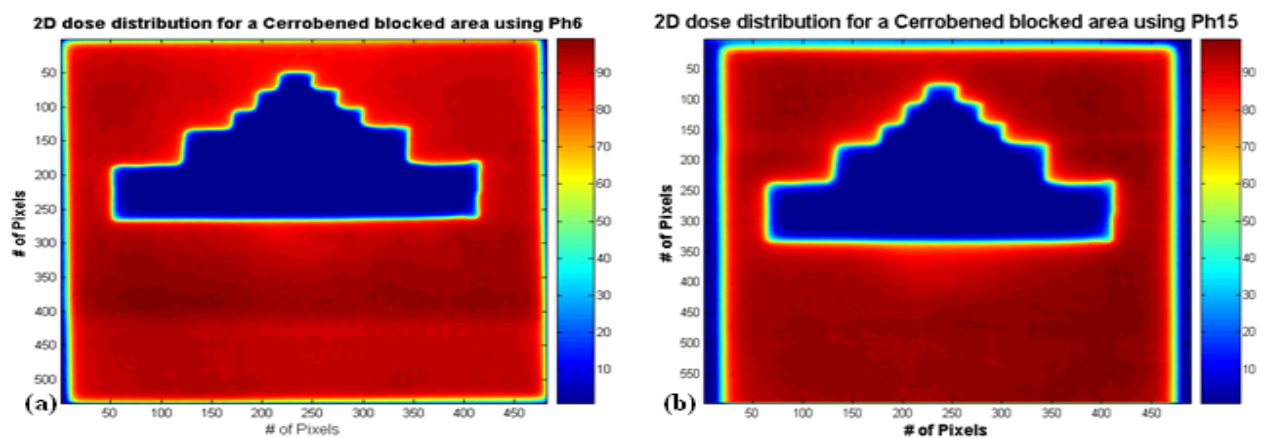


Figure 8. Two-dimensional dose distribution map for a stepped phantom Cerrobend block acquired using (a) 6 MV and (b) 15 MV photons.

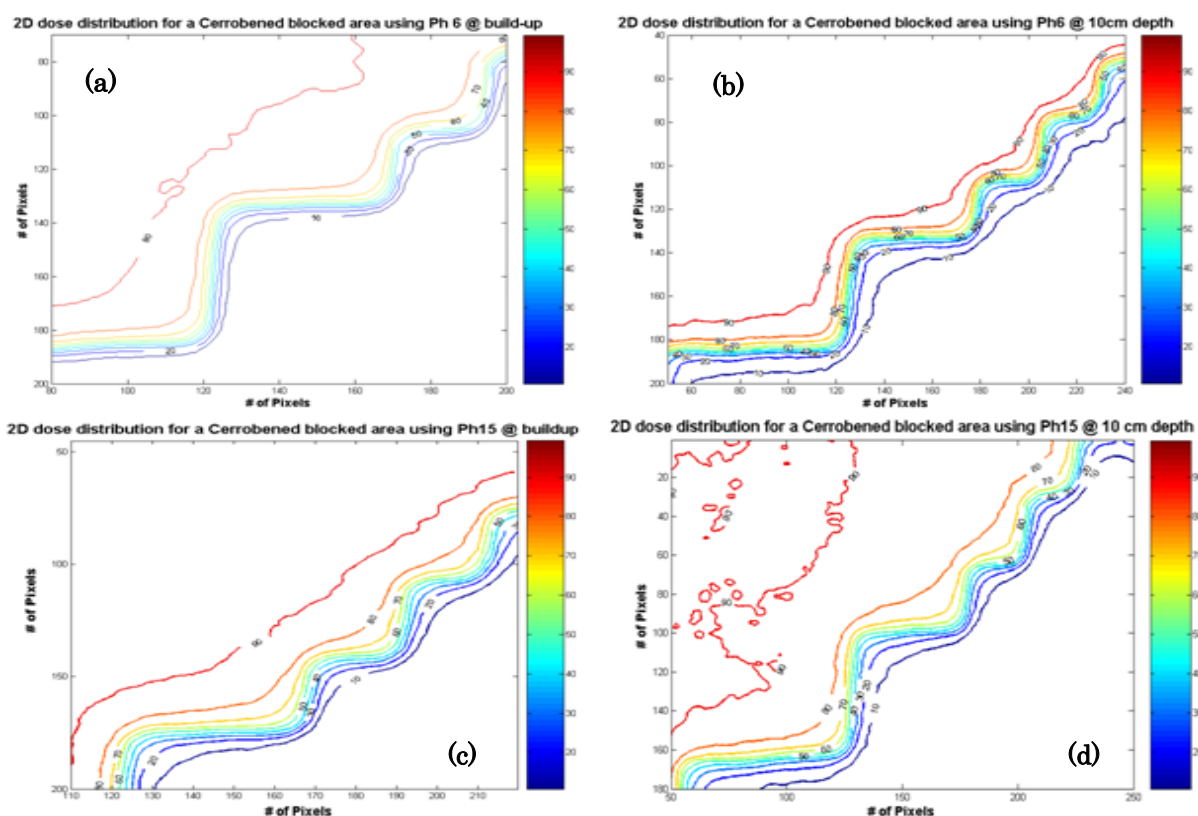


Figure 9. Magnified dose distribution contours for penumbra region for a stepped Cerrobend block acquired using EDR2 films for photon 6MV (a) at build-up layer (b) at 10-cm depth and for photon 15 MV (c) at build-up layer and (d) at 10-cm depth.

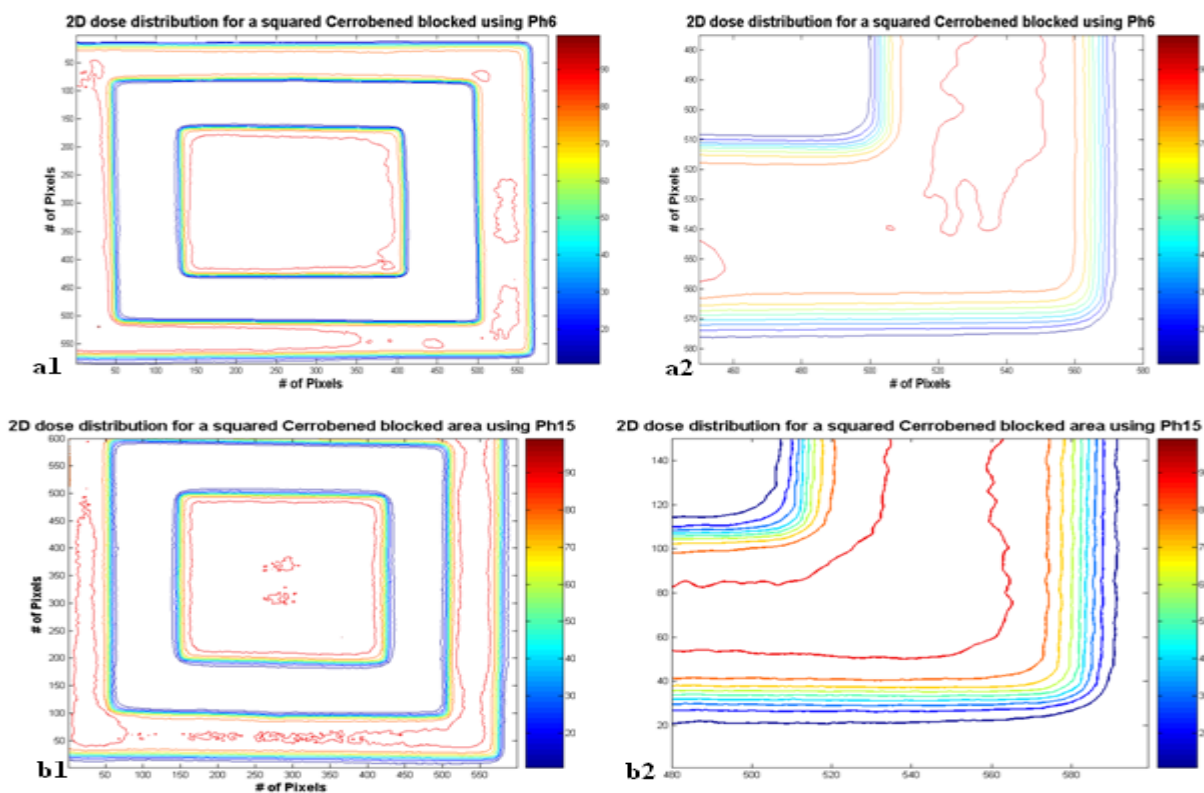


Figure 10. Relative isodose curves for a squared Cerrobend blocks for (a1) 6 MV and (b1) 15 MV photons and (a2 & b2) the corresponding magnified dose maps.

CONCLUSION

Cerrobend blocks are widely used in several radiation oncology centers to protect normal tissues. This study showed that regardless the Cerrobend disadvantages reported^(4, 8, 42), the advantages were recommended to be taken into consideration. However, further study is required to assess the dose distribution behind the protected area, as well as Cerrobend material modification during molding procedure.

REFERENCES

1. Johns HE and Cunningham JR (1983) The Physics of Radiology. 4th ed. American Lecture, Illinois: Charles Thomas. 796.
2. Khan FM (1993) The physics of radiation therapy. 3rd ed., Philadelphia: Lippincott Williams & Wilkins.
3. Muller-Runkel R, Ovadia J, Borger F et al. (1985) A shaping device for irregular electron fields for the Therac-20 accelerator. *Med Phys*, **12**: 90-2.
4. Ezzell GA, Orton CG, Maughan RL et al. (1987) Practical aspects of transmission cord blocks in radiotherapy. *Med Phys*, **14**: 400-5.
5. Famiglietti R, Noriega B, Sanders R (1990) A standardized block fabrication technique. *Med Dosim*, **15**: 151-8.
6. Wojcicka JB, Yankelevich R, Werner BL, Lasher DE. (2008) Technical note: on cerrobend shielding for 18-22 MeV electron beams. *Med Phys*, **35**: 4625-9.
7. Blackwell CR and Amundson KD (1990) Cadmium free lead alloy for reusable radiotherapy shielding. *Med Dosim*, **15**:127-9.
8. Boyer A, Biggs P, Galvin J, Klein E, LoSasso T, Low D, Mah K, Yu C, *Basic Application of Multileaf Collimators*. 2001, Task Group 50, AAPM: Madison.
9. Brahme A (1984) Dosimetric precision requirements in radiation therapy. *Acta Radiol Oncol*, **23**: 379-91.
10. Boyer AL, Ochrans TG, Nyerick CE, Waldron TJ, Huntzinger CJ. (1992) Clinical dosimetry for implementation of a multileaf collimator. *Med Phys*, **19**: 1255-61.
11. Frazier A, Yan D, Du M et al., (1995) Effects of treatment setup variation on beam's eye view dosimetry for radiation therapy using the multileaf collimator vs. the Cerrobend block. *Int J Radiat Oncol Biol Phys*, **33**: 1247-56.
12. Palta JR, Yeung DK, Frouhar V (1996) Dosimetric considerations for a multileaf collimator system. *Med Phys*, **23**: 1219-24.
13. Stasi M, Baiotto B, Palamara F, Gabriele P, Scielzo G. (1999) [Dosimetric characterization of a multileaf collimator]. *Radiol Med*, **97**: 382-8.
14. Pasquino M, Casanova Borca V, Tofani S (2001) Physical-dosimetric characterization of a multi-leaf collimator system for clinical implementation in conformational radiotherapy. *Radiol Med*, **101**: 187-92.
15. Hogstrom KR, Boyd RA, Antolak JA, Svatos MM, Faddegon BA, Rosenman JG (2004) Dosimetry of a prototype retractable eMLC for fixed-beam electron therapy. *Med Phys*, **31**: 443-62.
16. Cheng CW, Das IJ, and Steinberg T (2001) Role of multileaf collimator in replacing shielding blocks in radiation therapy. *Int J Cancer*, **96**: 385-95.
17. Galvin JM, Smith AR, Lally B (1993) Characterization of a multi-leaf collimator system. *Int J Radiat Oncol Biol Phys*, **25**: 181-192.
18. Jordan T and Williams P (1994) The design and performance characteristics of a multileaf collimator. *Phys Med Biol*, **39**: 231-51.
19. Butson M, Yu P, Cheung T (2003) Rounded end multileaf penumbral measurements with radiochromic film. *Phys Med Biol*, **48**: N247-52.
20. Klein E and Low D (2001) Interleaf leakage for 5 and 10 mm dynamic multileaf collimation systems incorporating patient motion. *Med Phys*, **28**: 1703-10.
21. Chow L, Seguin M, Alexander A (2005) Dosimetric effect of collimating jaws for small multileaf collimated fields. *Med Phys*, **32**: 759-765.
22. Huq MS, Yu Y, Chen ZP, Suntharalingam N. (1995) Dosimetric characteristics of a commercial multileaf collimator. *Med Phys*, **22**: 241-7.
23. Stasi M, Baiotto B, Palamara F, Gabriele P, Scielzo G. (1999) Dosimetric characterization of a multileaf collimator. *Radiol Med (Torino)*, **97**: 382-8.
24. Palta J, Yeung D, Frouhar V. (1996) Dosimetric consideration for a multileaf collimator system. *Med Phys*, **23**: 1219-24.
25. Klein E, Harms W, Low D, Willcut V, Purdy J. (1995) Clinical implementation of a commercial multileaf collimator: dosimetry, networking, simulation, and quality assurance. *Int J Radiat Oncol Biol Phys*, **33**: 1195-208.
26. Huq MS, Das IJ, Steinberg T, Galvin JM. (2002) A dosimetric comparison of various multileaf collimators. *Phys Med Biol*, **47**: N159-70.
27. Balog JP, Mackie TR, Wenman DL, Glass M, Fang G, Pearson D. (1999) Multileaf collimator interleaf transmission. *Med Phys*, **26**: 176-86.
28. Zhu Y, Boyer AL, Desobry GE. (1992) Dose distributions of x-ray fields as shaped with multileaf collimators. *Phys Med Biol*, **37**: 163-74.
29. Galvin JM, Leavitt DD, Smith AA. (1996) Field edge smoothing for multileaf collimators. *Int J Radiat Oncol Biol Phys*, **35**: 89-94.
30. Stasi M, Baiotto B, Palamara F, Gabriele P, Scielzo G. (2001) Effective penumbra and scalloping effect: a dosimetric study in multifield radiotherapy with multileaf collimator for prostate cancer treatment. *Tumori*, **87**: 30-5.
31. Cheng CW, Wong JR, Ndlovu AM, Das IJ, Schiff P, Uematsu M. (2003) Dosimetric evaluation and clinical application of virtual mini-multileaf collimator. *Am J Clin Oncol*, **26**: e37-44.
32. Liu Y, Shi C, Tynan P, Papanikolaou N (2008) Dosimetric characteristics of dual-layer multileaf collimation for small-field and intensity-modulated radiation therapy applications. *J Appl Clin Med Phys*, **9**: 2709.
33. Xu MM, Sethi A, Glasgow GP (2009) Dosimetry of small circular fields for 6-MeV electron beams. *Med Dosim*,

- 34: 51-6.
34. Childress N and Rosen I (2003) The design and testing of novel clinical parameters for dose comparison. *Int J Radiat Oncol Biol Phys*, **56**: 1464-79.
 35. Gerbi BJ and Dimitroyannis DA (2003) The response of Kodak EDR2 film in high-energy electron beams. *Med Phys*, **30**: 2703-5.
 36. Dogan N, Leybovich LB, Sethi A (2002) Comparative evaluation of Kodak EDR2 and XV2 films for verification of intensity modulated radiation therapy. *Phys Med Biol*, **47**: 4121-30.
 37. Zhu X, Jursinic P, Grimm D, Lopez F, Rownd J, Gillin M (2002) Evaluation of Kodak EDR2 film for dose verification of intensity modulated radiation therapy delivered by a static multileaf collimator. *Med Phys*, **29**: 1687-92.
 38. Mohammadi M, Bezak E, Reich P (2007) The use of extended dose range film for dosimetric calibration of a scanning liquid-filled ionization chamber electronic portal imaging device. *J Appl Clin Med Phys*, **8**: 69-84.
 39. Sankar A, Ayyangar KM, Nehru RM, Kurup PG, Murali V, Enke CA, Velmurugan J (2006) Comparison of Kodak EDR2 and Gafchromic EBT film for intensity-modulated radiation therapy dose distribution verification. *Med Dosim*, **31**: 273-82.
 40. Boyer A and Li S (1997) Geometric analysis of light-field position of a multileaf collimator with curved ends. *Med Phys*, **24**: 757-62.
 41. Dawson J, Kahler D, McDonald B, Kopecky W, Gu J (1997) Surface and percentage depth doses for secondary blocking using a multileaf collimator and cerrobend-alloy blocks. *Radiother Oncol*, **42**: 285-8.
 42. Du MN, Yu CX, Symons M, Yan D, Taylor R, Matter RC, Gustafson G, Martinez A, Wong JW (1995) A multileaf collimator field prescription preparation system for conventional radiotherapy. *Int J Radiat Oncol Biol Phys*, **32**: 513-20.

